Graphene Oxide Nanoplatforms to Enhance Catalytic Performance of Iron Phthalocyanine for Oxygen Reduction Reaction in Bioelectrochemical Systems

Maida Aysla Costa de Oliveira[a], Barbara Mecheri[a]*, Alessandra D'Epifanio[a], Ernesto Placidi[b,c], Fabrizio Arciprete[b], Federica Valentini[a], Alessando Perandini[d], Veronica Valentini[e], and Silvia Licoccia [a]*

[a] Department of Chemical Science and Technologies, University of Rome Tor Vergata, Via della Ricerca Scientifica, 00133 Rome, Italy.

[b] Department of Physics, University of Rome Tor Vergata, Via della Ricerca Scientifica, 00133 Rome, Italy.

[c] CNR-ISM, Via Fosso del Cavaliere 100, I-00133 Rome, Italy

[d] Department of Chemistry, Sapienza University of Rome, Piazzale Aldo Moro 2, 00185 Rome, Italy

[e] CNR-ISM, Via Salaria km 29.300, 00016 Monterotondo Scalo, Rome, Italy

[*] Corresponding authors :

Dr Barbara Mecheri

phone: +39 06 7259 4488; FAX: +39 06 7259 4328

email: barbara.mecheri@uniroma2.it

Prof. Silvia Licoccia

phone: +39 06 7259 4386; FAX: +39 06 7259 4328

email: licoccia@uniroma2.it

Abstract.

We report the development of electrocatalysts based on iron phthalocyanine (FePc) supported on graphene oxide (GO), obtained by electrochemical oxidation of graphite in aqueous solution of LiCl, $LiClO_4$, and $NaClO_4$. Structure, surface chemistry, morphology, and thermal stability of the prepared materials was obtained by Fourier transform infrared spectroscopy (FTIR), Raman spectroscopy, atomic force microscopy (AFM), thermogravimetric analysis (TGA), and X-ray photoelectron spectroscopy (XPS). The catalytic activity toward oxygen reduction reaction (ORR) at neutral pH was evaluated by cyclic voltammetry. The experimental results demonstrate that oxidation degree of GO supports affect the overall catalytic activity of FePc/GO, due to a modulation effect on the interactions between FePc and basal plane of GO. Among the three samples, FePc/GO_LiCl has the highest catalytic activity towards ORR, demonstrating good electrochemical performance in terms of voltage and power generation when assembled at the cathode side of a microbial fuel cell prototype.

Keywords: Graphene Oxide; Iron phthalocyanine; Oxygen reduction reaction; Bioelectrochemical Systems.

1. Introduction

Bioelectrochemical systems (BESs) can be considered as an innovative and flexible platform for integrated waste treatment and energy/resource recovery. All BESs share the same principle in the anode chamber where biodegradable substrates are oxidized by exoelectrogen bacteria during their anaerobic respiration. By diversifying the reaction at the cathode side, a great variety of applications have been developed, such as direct power generation (microbial fuel cells, MFCs), chemical production (microbial electrolysis cells, MECs; microbial electrosynthesis cells, MESs), or water

desalination (microbial desalination cells, MDCs) [1-4]. The extensive research work that have been devoted to this technology over the past decade demonstrates the promising outlook of BESs for highly efficient, energy-saving, and sustainable wastewater treatment [5-7]. On the other hand, practical application and widespread diffusion of BESs are still limited by the high costs associated to the materials used for device assembly, such as polymer separators [8] and mostly cathode materials which accounts for over 50% of the overall MFC capital cost [9]. The sluggish kinetics of oxygen reduction reaction (ORR) led to the use of expensive catalysts, such as platinum, to reduce the overpotential and accelerate ORR. On the other hand, platinum is not suitable to be applied to sustainable technologies due to its high cost and low natural abundance. It is then paramount to develop non precious ORR catalysts to boost performance of microbial fuel cells. A great variety of materials have been developed for MFC cathodes, including catalysts based on activated carbons (ACs) , metal–nitrogen–carbon (M-N-C) complexes, biocatalysts, and photoelectrocatalysts [10,11]. In particular, nitrogen-doped ACs and M-N-C catalysts allowed achieving ORR rate comparable to Pt, the morphology and structure of the catalysts playing an important role on the efficiency and durability of ORR active sites [12-16].

The development of new carbon nanostructures with highly tunable morphology and structure has led to the use of graphene for several applications, including as component for MFC cathodes [17,19]. It has been demonstrated that ORR is effectively catalyzed by graphene-based materials due to high density of active sites, high electrical conductivity, and ease of functionalization [20-22]. However, challenges, such as complexity in synthesis and high costs, still limit the applicability of graphene as cathode component of MFCs and other BESs.

Therefore, a facile and efficient approach to develop graphene based catalysts can be considered a promising direction to achieve sustainable water/wastewater treatment and bioenergy production by BESs.

In this paper, we report a facile method for large-scale preparation of ORR catalysts based on iron phthalocyanine (FePc) supported on graphene oxide (GO) obtained by electrochemical oxidation of graphite in aqueous solutions of different inorganic salts (MX). By using atomic force microscopy and electrochemical and spectroscopic techniques, we correlated the different morphology and surface chemistry of GO_MX supports with catalytic activity of FePc/GO_MX systems.

The investigation of the interactions between FePc and GO_MX provided key insights for the development of graphene-based electrocatalysts for BES application.

2. Experimental

2.1 Materials preparation

Graphite rods (diameter 10 mm, length 100 cm, particle size 21-100 μm and purity 99%) were purchased from Goodfellow. Carbon cloth with 30 wt.% PTFE wet-proofing was purchased by Quintech. Iron (II) phthalocyanine (FePc), Nafion perfluorinated resin solution (5 wt. % in lower aliphatic alcohols and water), and further chemicals were purchased from Aldrich.

GO preparation. Graphene oxide (GO) was prepared by electrochemical exfoliation of graphite. Two graphite rod electrodes (φ = 3 mm; L = 5cm) were immersed in a cell containing 80 mL of 0.1 M aqueous solution in MX salt (M= Li^+, Na^+, K^+; X= Cl^-, ClO_4^-), applying 24 V voltage for $6 \leq t \leq 22$h. Subsequently, the powder (labelled as GO_MX) was collected by drying the suspension in an oven at 70 °C overnight. GO_MX was further dispersed in distilled water (DI) to 1 mg/mL and centrifuged at 8500 rpm for 1 h. The supernatant was removed and GO was dried in an oven at 70 °C overnight .

Preparation of FePc/GO_MX catalysts. 0.5 g of FePc (Aldrich) were dissolved in 30 mL of methanol. 0.5 g of GO were added to the solution and the resulting mixture was stirred for 45 min. The mixture was heated in a water bath at 70 °C to evaporate methanol and the resulting powder was completely dried in an oven at 70 °C for 3 h, obtaining a product labeled as FePc/GO_MX.

2.2 Materials characterizations

Atomic Force Microscopy (AFM). AFM measurements were performed in air using a Veeco Multiprobe IIIa instrument. Experiments were carried out in tapping mode by using Si tips with a spring constant of about 40 N/m and a typical curvature radius on the tip of 7 nm. GO_MX was dispersed in DI to a 0.01 $mgmL^{-1}$ content and deposited on Mica substrates.

Fourier Transform Infrared Spectroscopy (FTIR). The chemical structure of GO was analyzed by FTIR using a Fourier transform infrared spectrometer (Type FTIR100, Perkin Elmer) in transmittance mode. GO_MX powder samples were pelleted in 150 mg of KBr using a Specac manual hydraulic press, by applying a pressure of 2 tons for 5 min. The diameter of pellets was 13 mm.

Raman Spectroscopy. Measurements were performed with a Raman spectrometer XY Dilor, recording the spectrum from 1200 to 2900 cm^{-1}, with resolution of 2c m^{-1}, using an excitation wavelength of 514.5 nm. The power of the laser beam is 3.5 mW, focused on the sample by using a 100X objective and performing 10 repetitions of 60 s, for each measurement. GO_MX was deposited on Si(111) surface, starting from 1 $mgmL^{-1}$ dispersion in isopropyl alcohol treated in an ultrasonic bath for 1 h.

X-ray Photoelectron Spectroscopy (XPS). XPS was performed using an Omicron DAR 400 Al/Mg Kα nonmonochromatized X-ray source, and a VG-CLAM2 electron spectrometer. GO_MX was dispersed in ethanol to a 1 $mgmL^{-1}$ content and deposited on silicon wafer.

Thermogravimetric Analysis (TGA). Thermal Analysis was performed by using a TGA/DSC1 Star System (Mettler Toledo), in N_2 with a heating rate of 5 °C/min.

Cyclic Voltammetry (CV). The catalytic activity towards ORR of the prepared materials was examined by cyclic voltammetry, using a VMP3 Potentiostat (Bio Logic Science Instruments) controlled by computer through EC-Lab V10.18 software. A conventional tree-electrode cell was used: the reference electrode was a saturated electrode calomel-SCE, Amel 303/SCG/12), the auxiliary electrode was a platinum wire (Amel, 805/SPG/12), and the working electrode (WE) was a glassy carbon disk (GC,

0.196 cm^2 area) modified with catalyst layer. Prior to measurements, GC was cleaned by diamond paste, washed with DI and treated in an ultrasonic bath in isopropanol for 15 minutes. CV experiments were carried out in 100 mM neutral phosphate buffer solution, saturated in nitrogen and oxygen atmosphere at room temperature. The potential window was +0.6 V ÷ -0.9 V and the scan rate 5 mVs^{-1}. Electrode surface electrical double-layer capacitance, C_{DL}, of was estimated by recording CV curves in an N_2-saturated atmosphere, with a scan rate range of 20–500 mVs^{-1}, and measuring the charging current at 0.4 V, in the absence of faradic contribution.[23-25].

The catalyst layer was prepared by dispersing 0.8 mg of FePc/GO_MX in 270 µL of DI and 135 µL of ethanol. This dispersion was treated in an ultrasonic bath for 30 min. Then, 50 µL of Nafion solution were added to the dispersion and vortexed for 2 minutes. 30 µL of the obtained dispersion were deposited on the GC electrode to a catalyst loading of 0.3 $mgcm^{-2}$ and dried at 70 °C for 12 min under vacuum.

2.3 Cathode preparation and characterization

MFC cathodes were prepared by modifying carbon cloth electrodes with two layers: the diffusion layer (exposed to air) and the catalyst layer (faced to MFC solution). The diffusion layer was prepared as previously described [26]. The deposition of the catalyst layer was carried out on the opposite side of the diffusion layer, by brushing a suspension prepared from 0.5 mgm^{-2} of FePc/GO_MX catalyst in 0.83 µL DI, 6,67 µL Nafion solution, and 3.33 µL isopropanoland. The electrodes were dried at room temperature for 24h. A standard Pt/C cathode was also prepared and used to assemble reference MFCs [27].

2.4 MFC fabrication and operation.

The electrochemical cell consisted in a single-chamber air-cathode MFC (inner volume: 28 mL) assembled as previously reported with a graphite fiber brush as anode and the modified carbon cloth as cathode (diameter 4 cm) [28]. MFCs were firstly acclimated as described before and fed with

phosphate buffer solution containing 1 gL^{-1} of sodium acetate. Polarization and power density curved were acquired by varying the external resistance (10-10000 Ω) every 30 min intervals and measuring the cell voltage at each resistance. All the measurements were carried out at room temperature (23 ± 3°C), three independent replicates for each cathode.

3. Results and Discussion

3.1 GO characterization

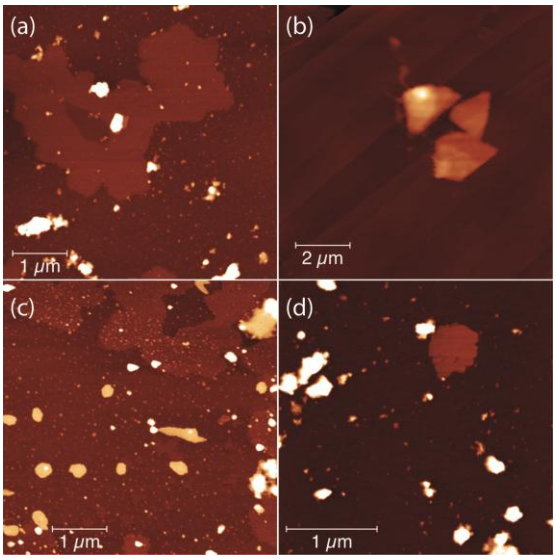

Fig. 1. AFM topographies of (a) GO_LiCl at high magnification, (b) GO_LiCl at low magnification, (c) GO_$LiClO_4$, and (d) GO_$NaClO_4$.

Fig. 1 shows the AFM topographies of GO_MX samples. For comparable areas, GO layers exhibit different situations. In GO_LiCl we find extended GO layers (10 μm^2 more) typically 1-4 monolayer (ML) high (Fig. 1a). Moreover, we partially observe the presence of very well oriented graphene sheets, having regular edges, as shown in Fig 1(b). Differently, in GO_$LiClO_4$ the GO layers exhibit surfaces generally smaller (0.03-0.15 μm^2) in average 3-4 ML high. Nonetheless, some wide GO layer (some μm^2) is somewhere present (Fig. 1c). In GO_$NaClO_4$ we could not find large GO layer, but only some small layer (0.03-0.25 μm^2), in average 3-4 ML high (Fig. 1d).

The information about oxygen-containing groups on the surface of GO_MX samples is obtained by FTIR Spectroscopy (Fig. 2a). For all samples, different functional groups are found in the FTIR spectrum, the most characteristic features being the bands at 1300-1000 cm^{-1} (C-O stretching vibrations from carboxyl and epoxide groups), 1720-1706 cm^{-1} (C=O stretching vibrations from carbonyl and

carboxyl groups), and 3570-3425 (O-H stretching vibrations). Hence, all GO_MX samples show a rich variety of transmittance bands due to carbonylic, carboxylic, epoxide, and hydroxylic groups, in good agreement with previous works [29].

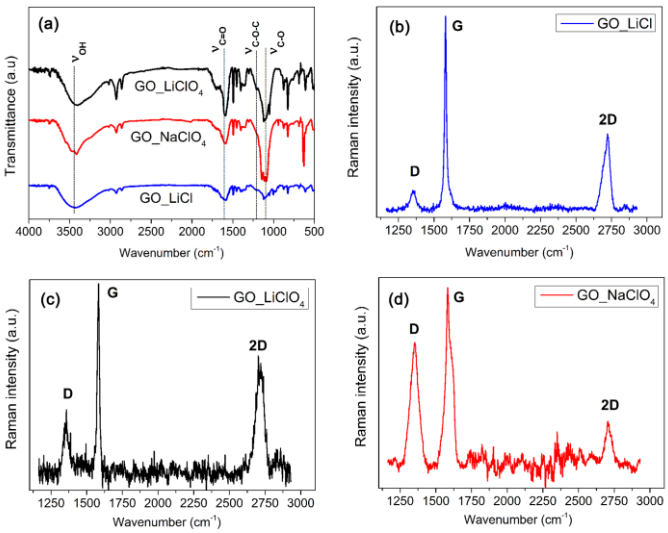

Fig. 2. FTIR Spectra of GO_MX samples (a); Raman spectrum of GO_LiCl (b), Raman spectrum of GO_LiClO_4 (c), and Raman spectrum of GO_NaClO_4 (d).

Fig. 2b shows the Raman profile of the GO_LiCl sample where a typical fingerprint of graphene is identified, especially for the presence of the 2D band that gives useful information about the number of the layers and demonstrates the conversion of the parent graphite into graphene [30]. Two layers are present in the case of sample GO_LiCl as obtained by curve fitting of the 2D bands (Table 1).

In the same spectral profile, there are also the typical G and D bands, that represent the graphite signal (centred around 1581.17 cm^{-1}, Table 1) and the defect band (D band centred around 1352.74 cm^{-1}, Table 1). The I_D/I_G ratio, also reported on Table 1, provides important information about the defects (in terms of the oxygenated functional groups) introduced on the graphene surfaces and edges, during the electrochemical exfoliation. For this sample, the content of defects (hence the functionalization degree) is very low leading to a regular morphology as highlighted by AFM results (Fig. 2b). The correlation

between the content of defects and the regularity in morphology of graphene sheets has been already observed in literature [31,32].

Fig. 2c shows the Raman profile for the GO_$LiClO_4$ film sample, having the typical graphene fingerprint. The I_{2D}/I_G ratio demonstrates the presence of 1 graphene layer (Table 1). The I_D/I_G ratio shows also a higher degree of defects, if compared with that obtained in presence of GO/LiCl film samples. These structure defects also explain the irregular shape of the GO/$LiClO_4$ sheets, as demonstrated by AFM micrograph shown in Fig. 2c.

Fig. 2d shows the Raman spectrum of GO_$NaClO_4$ This sample shows the lowest intensity of the 2D band, among the series of investigated samples. In addition, a lowest defect degree (see I_D/I_G ratio on Table 1) has been also recorded for GO_$NaClO_4$ film samples, indicating that a very poor functionalization degree was achieved during the electrochemical synthesis.

X-ray photoelectron spectra (XPS) is used to further clarify the surface composition and oxidation of graphene. The C1s spectra of GO_LiCl, GO_$LiClO_4$ and GO_$NaClO_4$ are shown in Fig. 3a, 3b, and 3c, respectively. The main peak (at binding energies around 284 eV) can be attributed to the graphitic C=C (aromatic) and C–C (aliphatic) oxygen-containing functional groups. The convolution of the C1s peak of three samples exhibits five peaks centered at higher binding energies (see Table 2), which can be assigned to the C (C–C, C=C), C–OH (hydroxyl), (C–O–C) epoxide, C=O (carbonyl) and C(O)O (carboxyl) functional groups respectively, and the peak p-p* assigned to p-electrons delocalized in the aromatic network.

XPS results indicate a remarkable extent of graphene oxidation. The clean C component is more intense in the GO_LiCl and GO_$NaClO_4$, while a higher content of carbon bound to hydroxyl, epoxide, carboxyl and carbonyl groups are found in GO_$LiClO_4$. This findings confirm the highest degree of oxidation of sample GO_$LiClO_4$, in agreement with FTIR and Raman analysis.

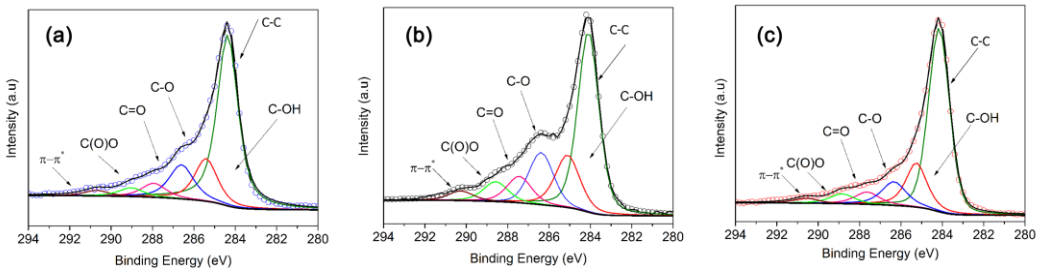

Fig. 3. C1s XPS spectra and related fit of (a) GO_LiCl, (b) GO_$LiClO_4$, and (c) GO_$NaClO_4$.

TGA is used to study the thermal stability of GO_MX and to assess the removal of bulk content of oxygen groups. Fig. 4 shows the TG curves and the corresponding DTG for GO_MX samples.

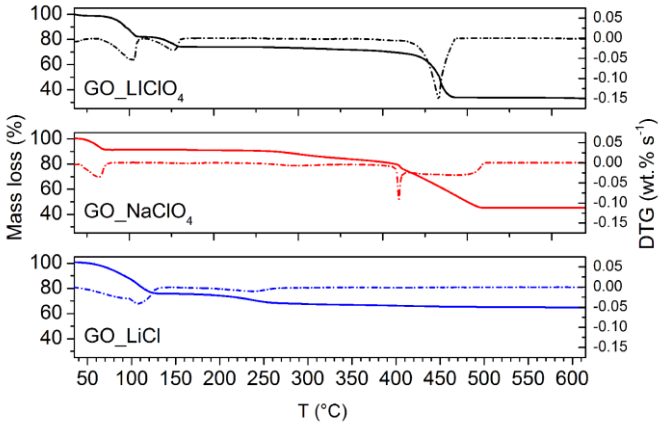

Fig. 4. Thermogravimetric (TG) and differential thermogravimetric (DTG) curves of GO_MX samples.

The samples exhibit up to three steps of mass losses associated to the desorption of physisorbed water (mass loss I, in the 25-115 °C range), the removal of oxygen-containing groups accompanied by the splitting-off of COx and H_2O molecules (mass loss II, in the 115-400°C range), and the combustion of residual perchlorates ions (mass loss III, in the 400-550°C range, absent for GO_LiCl sample).

Table 3 summarizes and compares the parameters obtained for all sample, such as weight loss percentage (wt.%), temperature range (T), and temperature of maximum rate of weight change (T_{MAX}).

The main differences in the TGA/DTG profiles reside in the lowest amount of physisorbed water of GO_$NaClO_4$ (mass loss I) and the lowest T_{MAX} of weight change in mass loss II for GO_$LiClO_4$. This can be associated to the low oxidation degree of GO_$NaClO_4$, and the high content of relatively more unstable oxygen functional groups of GO_$LiClO_4$, as highlighted by XPS results. Despite its low oxidation degree, the amount of physisorbed water of GO_LiCl is the highest among the GO series due to the high hygroscopicity of residual salt.

The catalytic activity towards ORR of the prepared samples is investigated by CV. While no peaks were detected under N_2 purging, all samples showed a reduction peak around -0.2 V, indicating catalytic activity towards ORR (Fig. S1). For the three samples, position and intensity of the peaks are very similar (about -0.2 V and -0.2 $mAcm^{-2}$, respectively), indicating that the morphology and oxidation degree of the supports have a negligible effect on ORR catalysis.

3.2 FePc/GO_MX characterization

To obtain highly active catalysts towards ORR, iron phthalocyanine is supported on GO_MX samples as described in the experimental (section 2.1). We acquire CVs of FePc/GO_MX samples in both N_2- and O_2 saturated electrolyte.

As indicated by Fig. 5, the deposition of iron phtalocianine on GO_MX supports results in a positive shift of the oxygen reduction potential and in an increase of peak current density with respect to GO_MX samples. The more positive potential and the higher current density of the oxygen reduction peak indicates the higher ORR activity of catalyst.

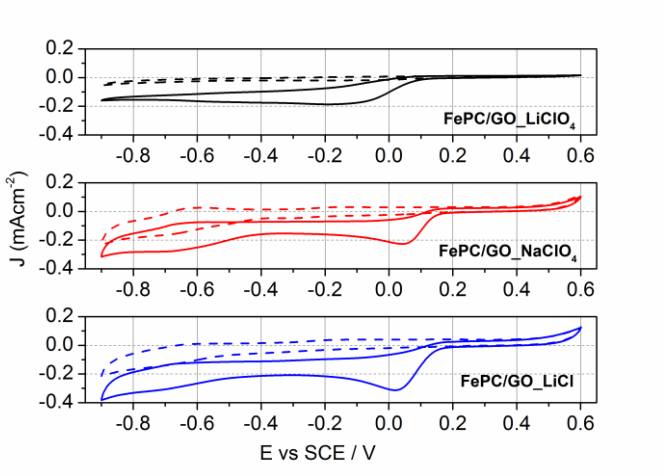

Fig. 5. Cyclic Voltammograms of FePc/GO_MX samples in N_2- (dashed lines) and O_2-saturated (solid lines) phosphate buffer solution.

Table 4 lists the E_{pr} (potential of oxygen reduction peak) and $|J_{pr}|$ (peak current density) for FePc/GO_MX samples and unsupported FePc taken as reference.

The enhanced catalytic activity of FePc/GO_MX samples arises from the coordination of iron, nitrogen (from FePc) and carbon (from both FePc and GO supports). As highlighted from previous works dealing with iron based catalysts supported on nanostructured carbon [15, 33], Fe-N-C moieties act as highly active catalytic sites for ORR catalyst. The poor catalytic activity of unsupported FePc can be ascribed to the overlap of catalytic sites and catalyst deactivation commonly associated with phthalocyanine aggregation [34]. The positive shift in E_{pr} and higher current density values clearly indicates that the interactions between FePc and GO_MX supports have a beneficial effect in preventing aggregation phenomena of FePc molecules, maintaining an open macromolecular structure, hence providing a higher density of active sites which significantly enhanced catalytic activity.

Among FePc/GO_MX samples, FePc/GO_$LiClO_4$ displays the poorest catalytic activity towards ORR. Such a feature can be ascribed to the high oxidation degree of GO_$LiClO_4$ sample, as indicated by the body of XPS, AFM, and TGA results, which might promote FePc aggregation.

To get deeper insight on this, we calculate the double-layer capacitance (C_{DL}) of electrical double layer formed at the FePc/GO_MX electrode–electrolyte interface upon application of DC voltage. The capacitance of this double layer depends on the structure and morphology of the electrode surface, and it is expected to increase with increasing the electrode surface area accessible to electrolyte ions [24, 35]. Unsupported FePc displays the lowest CDL value (Table 4), indicating the lowest surface area accessible to electrolyte ions due to the above-mentioned aggregation phenomena. When FePc was supported on GO_MX, C_{DL} increased in the series FePc/GO_$LiClO_4$ « FePc/GO_$NaClO_4$ < FePc/GO_LiCl indicating that the supports affects the electrocatalysts surface area; in particular, GO_LiCl allows FePc to exhibit the highest surface area while GO_$LiClO_4$ the lowest one. Hence, the good electrocatalytic activity of FePc/GO_LiCl towards ORR can be ascribed to the low content of defect/low oxidation degree, high exfoliation degree, and high regularity of GO_LiCl support which guarantee a high density of active sites.

Given this promising feature, FePc/GO_LiCl is selected to deepen the investigation and to get insights on the nature of Fe-C-N active sites.

Morphology of this sample consists in large single layer graphene sheets (with area of several μm^2) with many 3-4 layer smaller sheets (Fig. 6a).

Fig. 6b shows the FTIR spectra of FePc and FePc/GO_LiCl together with that of GO_LiCl. The spectrum of unsupported FePc spectrum shows stretching and bending vibration bands typical of metal phthalocyanines, including vibrations of nitrogen bridging atoms (1512 cm^{-1}), stretching vibrations of isoindole (1434 cm^{-1}) and pyrrole (1335 cm^{-1}), and in plane C-H bending (1288, 1164, 1119, 1083 cm^{-1}) [36, 37].

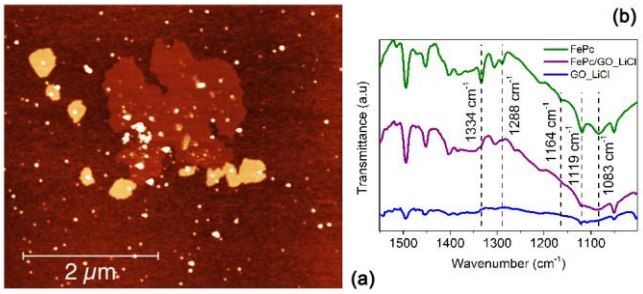

Fig 6. AFM micrograph of FePc/GO_LiCl (a) and FTIR Spectra of FePc, FePc/GO_LiCl, and GO_LiCl sample (b)

When supported on GO_LiCl, FePc shows several differences in the stretching and bending vibration bands. As highlighted by the dashed lines in Fig. 8b, the vibration band at 1334 cm^{-1} disappears, while the intensity of those at 1288, 1164, and 1119 cm^{-1} strongly decreases, turning into a shoulder. Moreover, the band at 1083 cm^{-1} become broader. Such differences in the FTIR spectra of FePc and FePc/GO_LiCl can be ascribed to interactions between phthalocyanine and the basal plane of graphene via π-π stacking [38].

XPS measurements are also performed to get further insights on FePc/GO interaction.

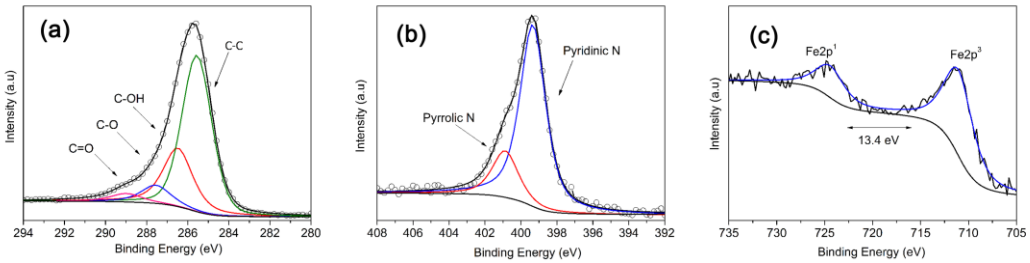

Fig. 7. XPS spectra of GO_LiCl_FePc (a) C1s (b) N1s, and (c) Fe2p.

Fig. 7 shows the spectra and relative fits for C, N, and Fe core peaks. Atomic percentage of C-C oxygen groups slightly increased in comparison with the same sample without the FePc and N 1s peak

exhibits two components corresponding, both in energy and intensity ratio, to the two coordination of nitrogen atoms in the phthalocyanine (Pc), including pyridinic/pyrrolic nitrogen (table 5). In nitrogen-containing carbon materials, it is believed that either pyridinic or pyrrole/pyridone type nitrogen is responsible for the enhanced ORR activity [15, 39, 40]. Fe 2p spectra exhibit a single component that correspond to a 3^{+} valence, that is a possible oxidation state of iron. High oxidation states of a metal are known to facilitate reductive O-O cleavage [41].

3.3 MFC tests

FePc/GO_LiCl is then assembled as cathode in MFC prototypes to evaluate its electrochemical performance in terms of voltage and power generation.

Fig. 8a shows the voltage generation cycles of cells assembled with FePc/GO_LiCl and reference Pt/C as a function of time. MFC assembled with Pt/C as cathode generates high and stable voltage in the first cycles (0.57 V during 350 hours), then voltage progressively decreases due to the well known Pt deactivation and poisoning in the presence of typical MFC metabolites [42]. By contrast, MFC assembled with FePc/GO_LiCl generates low voltage in the first cycles, but the voltage progressively increases becoming stable after ca. 350 h of operation and remaining stable and and higher than that of Pt/C up to 550 h.

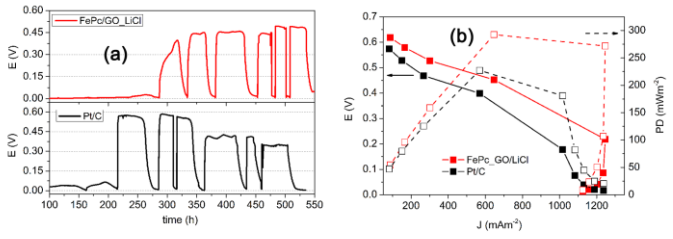

Fig. 8. (a) Voltage cycles under a 1 kV external resistance recorded for 550 h from inoculation and (b) cell voltage (E) and power density (PD) of MFCs assembled with FePc/GO_LiCl and Pt/C cathodes and fed with 1 mgL^{-1} sodium acetate in neutral phosphate buffer.

Polarization and power density (PD) curves of MFCs assembled with FePc/GO_LiCl and Pt/C are acquired after 550 h from inoculation The cell assembled with FePc/GO_LiCl as cathode reaches a maximum power density of 295 mWm^{-2}, corresponding to 1.2 Am^{-2} current density. The performance is similar and even higher than that of the MFC assemble with reference Pt/C as cathode. Moreover, electricity and power generation are consistent with existing literature reporting the performance of MFCs assembled with cathodes based either on graphene or metal phthalocyanines supported on different types of nanostructured carbon [43-50]. It should however be noted that the use of nanostructured carbon as catalyst support generally implies time consuming and expensive post treatments (*i.e.*, thermal annealing and/or doping with heteroatom functionalities) to boost catalytic activity. By contrast, supporting FePc on GO_LiCl allowed generating considerable power density, without any post treatment. This points out that FePc/GO_LiCl has the added value of guaranteeing good performance while reducing the device costs, hence being a suitable candidate to substitute platinum as catalysts at the cathode side of bioelectrochemical systems.

4. Conclusions

We reported a facile method for large-scale preparation of ORR catalysts based on iron phthalocyanine (FePc) supported on graphene oxide (GO) obtained by electrochemical oxidation of graphite in aqueous solutions of LiCl, $LiClO_4$, and $NaClO_4$.

The electrochemical exfoliation of graphite allowed obtaining completely exfoliated GO nanosheets, decorated with carbonylic, carboxylic, epoxide, and hydroxylic surface functionalities, as highlighted by FTIR, Raman, XPS, and TGA results. In particular, the analysis of Raman and XPS spectra provided insights on the exfoliation and oxidation degree of the samples. The exfoliation degree was more pronounced for GO_$LiClO_4$ and GO_LiCl, compared to GO_$NaClO_4$. Moreover, the highest

content of defects (in terms of oxygenated functional groups) introduced on graphene surfaces and edges was found in GO_$LiClO_4$, while for GO_LiCl and GO_$NaClO_4$ the degree of functionalization was lower. The high exfoliation degree and the low content of defects for GO_LiCl resulted in very well oriented graphene sheets with regular edges, as indicated by AFM micrographs.

The GO nanosheets were used as support for FePc; AFM, and FTIR analysis brought to light the interaction between phthalocyanine and basal plane of graphene via π-π stacking.

The catalytic activity towards ORR of FePc/GO systems was evaluated by cyclic voltammetry. FePc/GO_$LiClO_4$ sample displayed the poorest catalytic activity towards ORR due to the high oxidation degree of GO support, which promotes FePc aggregation. By contrast, FePc/GO_LiCl displayed good electrocatalytic activity of towards ORR due to the low content of defect/low oxidation degree, high exfoliation degree, and high regularity of GO_LiCl support which guarantee a high density of active sites. Moreover, the analysis of C, N, an Fe XPS spectra of FePc/GO_LiCl revealed the pyridinic/pyrrolic coordination of nitrogen atoms and Fe(III) as oxidation state of iron, both the features being responsible for the high ORR activity.

To demonstrate the applicability of FePc/GO_LiCl as ORR catalysts in bioelectrochemical systems, we assembled FePc/GO_LiCl at the cathode side of a microbial fuel cell (MFC) prototype. MFCs assembled with FePc/GO_LiCl generated stable voltage cycles and considerable power density, while reduced the device costs compared to reference Pt/C cathodes. This points at FePc/GO_LiCl as suitable candidate to substitute platinum as catalysts at the cathode side of bioelectrochemical systems.

Acknowledgements

The present work was carried out with the support of the "European Union's Horizon 2020 research and innovation programme", under H2020-FTIPilot-2015-1 (Grant Agreement n. 720367-GREENERNET) and "CNPq - Conselho Nacional de Desenvolvimento Científico e Tecnológico",

Brazil. Thanks are due to Ms. Cadia D'Ottavi (Dept of Chemical Science and Technologies, University of Rome Tor Vergata) and Mr Giuseppe Piciacchia (CNR-ISM, Monterotondo) for their valuable technical support.

References

[1] X. Chen, P. Liang, X. Zhang, X. Huang, Bioelectrochemical Systems-Driven Directional Ion Transport Enables Low-Energy Water Desalination, Pollutant Removal, And Resource Recovery, Bioresource Technol. 215 (2016) 274-284.

[2] A. Rinaldi, B. Mecheri, V. Garavaglia, S. Licoccia, P. Di Nardo, E. Traversa, Engineering Materials And Biology To Boost Performance Of Microbial Fuel Cells: A Critical Review, Energ. Environ. SCI. 1 (2008) 417-429.

[3] H. Nie, T. Zhang, M. Cui, H. Lu, D.R. Lovley, T.P Russell, Improved Cathode For High Efficient Microbial-Catalyzed Reduction In Microbial Electrosynthesis Cells, Phys. Chem. Chem. Phys. 15 (2013) 14290-14294.

[4] S. Sevda, H. Yuan, Z. He, I.M. Abu-Reesh, Microbial Desalination Cells As A Versatile Technology: Functions, Optimization And Prospective, Desalination. 371(2015) 9-17.

[5] A. ElMekawy, S. Srikanth, S. Bajracharya, H.M. Hegab, P.S. Nigam, A. Singh, S.V. Mohan, D.Pant, Food And Agricultural Wastes As Substrates For Bioelectrochemical System (Bes): The Synchronized Recovery Of Sustainable Energy And Waste Treatment, Food Res. Int. 73 (2015) 213-225.

[6] S.M Iskander, B. Brazil, J.T. Novak, Z. He, Resource Recovery From Landfill Leachate Using Bioelectrochemical Systems: Opportunities, Challenges, And Perspectives, Bioresource Technol. 201(2016) 347-354.

[7] D. Pant, A. Singh, G. Van Bogaert, S. Irving Olsen, P. Singh Nigam, L Diels, K. Vanbroekhoven, Bioelectrochemical Systems (Bes) For Sustainable Energy Production And Product Recovery From Organic Wastes And Industrial Wastewaters, RSC Adv. 2 (2012) 1248-1263.

[8] S. Angioni, L. Millia, G. Bruni, C. Tealdi, P. Mustarelli, E. Quartarone, Improving The Performances Of Nafion™-Based Membranes For Microbial Fuel Cells With Silica-Based, Organically-Functionalized Mesostructured Fillers, J Power Sources. 334 (2016) 120-127.

[9] R.A. Rozendal, H.V.M. Hamelers, K. Rabaey, J. Keller, C.J.N. Buisman, Towards Practical Implementation Of Bioelectrochemical Wastewater Treatment, Trends. Biotechnol. 26 (2008) 450–459.

[10] H.Yuan, Y. Hou, I.M. Abu-Reesh, J. Chen, Z. He, Oxygen Reduction Reaction Catalysts Used In Microbial Fuel Cells For Energy-Efficient Wastewater Treatment: A Review, Mater. Horiz. 3 (2016) 382-401.

[11] A. G.Campo, P. Cañizares, M. A. Rodrigo, F. J. Fernández, J. Lobato, Microbial Fuel Cell With An Algae-Assisted Cathode: A Preliminary Assessment, J Power Sources. 242 (2013) 638-645.

[12] W. Yang, B. E. Logan, Immobilization Of A Metal-Nitrogen-Carbon Catalyst On Activated Carbon With Enhanced Cathode Performance In Microbial Fuel Cells, ChemSusChem. 9 (2016) 1-8.

[13] M.T. Nguyen, B. Mecheri, A. D'Epifanio, T.P. Sciarria, F. Adani, S. Licoccia, Iron Chelates As Low-Cost And Effective Electrocatalyst For Oxygen Reduction Reaction In Microbial Fuel Cells, Int J Hydrogen Energ. 39 (2014) 6462-6469.

[14] M.T. Nguyen, B. Mecheri, A. Iannaci , A. D'Epifanio, T.P. Sciarria, F. Adani, S. Licoccia, Iron/Polyindole-Based Electrocatalysts To Enhance Oxygen Reduction In Microbial Fuel Cells, Electrochim. Acta. 190 (2016) 388-395.

[15] A. Iannaci, B. Mecheri, A. D'Epifanio, M. J. Lázaro Elorri, S. Licoccia, Iron–Nitrogen-Functionalized Carbon As Efficient Oxygen Reduction Reaction Electrocatalyst In Microbial Fuel Cells, Int J Hydrogen Energ. 41 (2016) 19637-19644.

[16] C. Santoro, A. Serov, L. Stariha, M. Kodali, J. Gordon, S. Babanova, O. Bretschger, K. Artyushkova, P. Atanassov, Iron Based Catalysts From Novel Low-Cost Organic Precursors For

Enhanced Oxygen Reduction Reaction In Neutral Media Microbial Fuel Cells, Energ. Environ. Sci. 9 (2016) 2346-2353.

[17] D. Torres, J.L. Pinilla, R. Moliner, I. Suelves, On The Oxidation Degree Of Few-Layer Graphene Oxide Sheets Obtained From Chemically Oxidized Multiwall Carbon Nanotubes, Carbon. 81(2015) 405-417.

[18] H. Yuan, Z. He, Graphene-Modified Electrodes For Enhancing The Performance Of Microbial Fuel, Nanoscale. 7 (2015) 7022-7029.

[19] M.V. Kannan, G. Gnana kumar, Current Status, Key Challenges And Its Solutions In The Design And Development Of Graphene Based Orr Catalysts For The Microbial Fuel Cell Applications, Biosens. Bioelectron. 77 (2016) 1208-1220.

[20] L. Feng, Y. Chen, L. Chen, Easy-to-Operation and Low-Temperature Synthesis of Gram-Scale Nitrogen-Doped Graphene and Its Application as Cathode Catalyst in Microbial Fuel Cells, ACS Nano. 5 (2011) 9611–9618.

[21] K. Parvez, S. Yang, Y. Hernandez, A. Winter, A. Turchanin, X. Feng, K. Müllen, Nitrogen-Doped Graphene And Its Iron-Based Composite As Efficient Electrocatalysts For Oxygen Reduction Reaction, ACS Nano. 6 (2012) 9541-9550.

[22] Y. Liu, H. Liu, C. Wang, S.X. Hou, N. Yang, Sustainable Energy Recovery In Wastewater Tratment By Microbial Fuel Cells: Stable Power Generation With Nitrogen-Doped Graphene Cathode, Environ. Sci. Technol. 47 (2013), 13889–13895.

[23] L.M Da Silva, L.A De Faria, J.F.C Boodts, Determination Of The Morphology Factor Of Oxide Layers, Electrochim. Acta. 47 (2001) 395-403.

[24] B.Mecheri, A. Iannaci, A. D'Epifanio, A. Mauri, S. Licoccia, Carbon-Supported Zirconium Oxide As A Cathode For Microbial Fuel Cell Applications, ChemPlusChem. 81 (2016) 80-85.

[25] V. Thirumal, A. Pandurangan, R. Jayavel, R. Ilangovan, Synthesis And Characterization Of Boron Doped Graphene Nanosheets For Supercapacitor Applications, Synthetic Met. 220 (2016) 524-532.

[26] A. Iannaci, T. Pepè Sciarria, B.Mecheri, F. Adani, S. Licoccia, A. D'Epifanio, Power Generation Using A Low-Cost Sulfated Zirconium Oxide Based Cathode In Single Chamber Microbial Fuel Cells, J Alloys Compd. 693 (2017) 170-176.

[27] T. Pepe Sciarria, G. Merlino, B. Scaglia, A. D'Epifanio, B. Mecheri, S. Borin, S. Licoccia, F. Adani. Electricity Generation Using White And Red Wine Lees In Air Cathode Microbial Fuel Cell, J Power Sources. 274 (2015) 393-399.

[28] T.P, Sciarria, A. Tenca, A. D'Epifanio, B. Mecheri, G. Merlino, M. Barbato, S. Borin, S. Licoccia, V. Garavaglia, F. Adani, Using Olive Mill Wastewater To Improve Performance In Producing Electricity From Domestic Wastewater By Using Single-Chamber Microbial Fuel Cell, Bioresource Technol. 147 (2013) 246-253.

[29] G. Zhao, J. Li, X. Ren, C. Chen, and X. Wang, Few-Layered Graphene Oxide Nanosheets As Superior Sorbents For Heavy Metal Ion Pollution Management, Environ. Sci. Technol. 45 (2011) 10454–10462.

[30] A. C. Ferrari, Raman Spectroscopy Of Graphene And Graphite: Disorder, Electron–Phonon Coupling, Doping And Nonadiabatic Effects, Solid State Commun.143 (2007) 47–57.

[31] C. Casiraghi, A. Hartschuh, H. Qian, S. Piscanec, C. Georgi, A. Fasoli, K. S. Novoselov, D. M. Basko and A.C. Ferrari, Raman Spectroscopy Of Graphene Edges, Nano Lett. 9 (2009) 1433–1441.

[32] S.d Eigler, F. Hof, M.E. Heim, S. Grimm, P. Müller, A. Hirsch, Statistical Raman Microscopy And Atomic Force Microscopy On Heterogeneous Graphene Obtained After Reduction Of Graphene Oxide, J Phys. Chem. C. 118 (2014) 7698–7704.

[33] C. Santoro, A. Serov, C.W. Narvaez Villarrubia, S. Stariha, S. Babanova, A.J. Schuler, K. Artyushkova, P. Atanassov, Double-Chamber Microbial Fuel Cell With A Non-Platinum-Group Metal Fe-N-C Cathode Catalyst, ChemSusChem. 8 (2015) 828-834.

[34] M. Pirouzmand, M.M Amini, N. Safari, Immobilization Of Iron Tetrasulfophthalocyanine On Functionalized Mcm-48 And Mcm-41 Mesoporous Silicas: Catalysts For Oxidation Of Styrene, J Colloid. Interf. Sci. 319 (2008) 199-205.

[35] L-H. Wang, M. Toyoda, M. Inagaki, Dependence Of Electric Double Layer Capacitance Of Activated Carbons On The Types Of Pores And Their Surface Areas, New Carbon Mater. 23 (2008) 111-115.

[36] A.V. Ziminov, S.M. Ramsh, E.I. Terukov, I.N. Trapeznikova, V.V. Shamanin, T.A. Yurr, Correlation Dependences In Infrared Spectra Of Metal Phthalocyanines, Semiconductors. 40 (2006) 1131- 1136.

[37] A. Monteverde Videla, L. Osmieri, M. Armandi, S. Specchia, Varying The Morphology Of Fe-N-C Electrocatalysts By Templating Iron Phthalocyanine Precursor With Different Porous Sio2 To Promote The Oxygen Reduction Reaction, Electrochim. Acta. 177 (2015) 43-50.

[38] C. Zhang, R. Hao, H. Yin, F. Liu, Y. Hou, Iron Phthalocyanine And Nitrogen-Doped Graphene Composite as a Novel Non-Precious Catalyst for the Oxygen Reduction Reaction, Nanoscale. 4 (2012) 7326- 7329.

[39] H.C. Nagaiah, S. Kundu, M. Bron, M. Muhler, W.Schuhmann, Nitrogen-Doped Carbon Nanotubes As a Cathode Catalyst For The Oxygen Reduction Reaction in Alkaline Medium, Electrochem. Commun. 12 (2010) 338-341.

[40] C. Santoro, A. Serov, R. Gokhale, S. R. Carbonell, L. Stariha, J. Gordon, K. Artyushkova, P. Atanassov, A Family Of Fe-N-C Oxygen Reduction Electrocatalysts For Microbial Fuel Cell (MFC)

Application: Relationships Between Surface Chemistry And Performances, Appl. Catal. B: Environ. 205 (2017) 24-33.

[41] A Mahammed, M. Kosa, D.T. Major, Z. Gross, L. Elbaz, Metallocorroles As Nonprecious‐Metal Catalysts For Oxygen Reduction N Levy Angew, Chem. Int. Edit. 54 (2015) 14080-14084.

[42] U. Schröder, J. Nießen and F. Scholz, A Generation Of Microbial Fuel Cells With Current Outouts Boosted By More Than One Order Of Magnitude Angew, Chem. Int. Ed. 42 (2003) 2880–2883.

[43] Y. Ren, D. Pan, X. Li, F. Fu, Y. Zhao, X. Wang, Effect Of Polyaniline-Graphene Nanosheets Modified Cathode On The Performance Of Sediment Microbial Fuel Cell, J Chem. Technol. Biotechnol. 88 (2013) 1946-1950.

[44] Y.Yuan, J. Ahmed, S. Kim, Polyaniline/Carbon Black Composite-Supported Iron Phthalocyanine As An Oxygen Reduction Catalyst For Microbial Fuel Cells. J Power Sources .196 (2011) 1103-1106.

[45] Y. Yuan, B. Zhao, Y. Jeon, S. Zhong, S. Zhou, S. Kim, Iron Phthalocyanine Supported On Amino-Functionalized Multi-Walled Carbon Nanotube As An Alternative Cathodic Oxygen Catalyst In Microbial Fuel Cells, Bioresource Technol. 102 (2011) 5849-5854.

[46] B. Li, X. Zhou, X., Wang, B. Liu, B. Li, Hybrid Binuclear-Cobalt-Phthalocyanine As Oxygen Reduction Reaction Catalyst In Single Chamber Microbial Fuel Cells, J Power Sources. 272 (2014) 320-327.

[47] J. Ahmed, H.J. Kim, S. Kim, Embedded Cobalt Oxide Nano Particles On Carbon Could Potentially Improve Oxygen Reduction Activity Of Cobalt Phthalocyanine And Its Application In Microbial Fuel Cells, RSC Advances. 4 (2014) 44065-44072.

[48] B. Li, M. Wang, X. Zhou, X.Wang, B.Liu, B. Li, Pyrolyzed Binuclear-Cobalt-Phthalocyanine As Electrocatalyst For Oxygen Reduction Reaction In Microbial Fuel Cells, Bioresource Technol. 193 (2015) 545-548.

[49] M. Ghasemi, W.R.W Daud, M. Rahimnejad, M. Rezayi, A. Fatemi, Y. Jafari, M.R. Somalu, A. Manzour, Copper-Phthalocyanine And Nickel Nanoparticles As Novel Cathode Catalysts In Microbial Fuel Cells, Int. J Hydrogen Energ. 38 (2013) 9533-9540.

[50] J. Ahmed, Y. Yuan, L. Zhou, S. Kim, Carbon Supported Cobalt Oxide Nanoparticles-Iron Phthalocyanine As Alternative Cathode Catalyst For Oxygen Reduction In Microbial Fuel Cells, J Power Sources. 208 (2012) 170-175.

Figures captions

Fig 1. AFM topographies of (a) GO_LiCl at high magnification, (b) GO_LiCl at low magnification, (c) GO_$LiClO_4$, and (d) GO_$NaClO_4$.

Fig. 2. FTIR spectra of GO_MX samples (a); Raman spectrum of GO_LiCl (b), Raman spectrum of GO_$LiClO_4$ (c), and Raman spectrum of GO_$NaClO_4$ (d).

Fig. 3. C1s XPS spectra and related fit of (a) GO_LiCl, (b) GO_$LiClO_4$, and (c) GO_$NaClO_4$.

Fig. 4. Thermogravimetric (TG) and differential thermogravimetric (DTG) curves of GO_MX samples.

Fig. 5. Cyclic Voltammograms of FePc/GO_MX samples in N_2- (dashed lines) and O_2-saturated (solid lines) phosphate buffer solution.

Fig. 6. (a) AFM micrographs of FePc/GO_LiCl and (b) FTIR Spectra of FePc, FePc/GO_LiCl, and GO_LiCl samples.

Fig. 7. XPS spectra of GO_LiCl_FePc (a) C1s (b) N1s and (c) Fe2p.

Fig. 8. (a) Voltage cycles under a 1 kV external resistance recorded for 550 h from inoculation and (b) cell voltage (E) and power density (PD) of MFCs assembled with FePc/GO_LiCl and Pt/C cathodes and fed with 1 mgL^{-1} sodium acetate in neutral phosphate buffer.

Tables

Table 1: Raman parameters for GO_LiCl, GO_$LiClO_4$, and GO_$NaClO_4$ samples.

Samples	**Frequency (cm^{-1})**	**Assigned Bands**	**I_D/I_G**	**I_{2D}/I_G**
GO_LiCl	2726.48	$2D_2$	0.09	0.31
	2692.18	$2D_1$		
	1581.17	G		N.of layers:5
	1352.74	D		
GO_$LiClO_4$	2713.15	$2D_1$	0.27	0.57
	1581.96	G		
	1356.75	D		N.of layers:1
GO_$NaClO_4$	2708.74	$2D_1$	0.02	0.22
	1615.01	D’		
	1583.60	G		N.of layers:5
	1553.35	G		
	1379.97	D		
	1350.87	D		

Table 2: Atomic percentage from XPS C1s fit for GO_LiCl, GO_$LiClO_4$, and GO_$NaClO_4$.

Peak BE (eV)	**Species**	**GO_LiCl At%**	**GO_$LiClO_4$ At%**	**GO_$NaClO_4$ At%**
284.4	C-C	59.0	50.0	61.0
285.4	C-OH	16.0	18.0	17.0
286.6	C-O	14.0	16.0	11.0
287.7	C=O	7.0	9.0	7.0
289.0	C(O)O	4.0	7.0	4.0

Table 3: Weight loss percentage (wt.%), temperature range (T), and temperature of maximum rate of weight change (T_{MAX}) from TG/DTG analysis of Go_LiCl, GO_$LiClO_4$, and GO_$NaClO_4$.

Parameter	**GO_LiCl**	**GO_$LiClO_4$**	**GO_$NaClO_4$**
Mass loss I			
wt.%	25.0	17.8	8.6
T °C	25 – 140	25 – 115	25 – 115
T_{max}	106	102	63
Mass loss II			
wt.%	9.7	9.5	10
T °C	140 - 400	115 - 250	115 - 400
T_{max}	237	153	300
Mass loss III			
wt.%	-	40.0	36.3
T °C	-	250 – 550	400 – 550
T_{max}	-	466	419

Table 4: E_{pr} (potential of oxygen reduction peak), $|J_{pr}|$ (peak current density), and C_{DL} (double layer capacitance) for FePc and FePc/GO_MX samples.

Sample	**E_{pr} / V**	**J_{pr} / mAcm^{-2}**	**C_{DL} / Fm^{-2}**
FePc	-0.597	0.175	1.96
FePc/GO_LiCl	0.027	0.366	21.2
FePc/GO_$LiClO_4$	-0.076	0.182	5.02
FePc/GO_$NaClO_4$	0.049	0.198	20.3

Table 5: Atomic percentage from XPS C1s, and N1s fit of FePc/GO_LiCl.

Peak BE (eV)	**Species**	**At%**
285.5	C-C	66.0
286.5	C-OH	18.6
287.6	C-O	11.0
289.0	C=O	4.4
399.3	Pyridinic N	78.0
400.9	Pyrrolic N	22.0

Figure captions

Fig 1. AFM topographies of (a) GO_LiCl at high magnification, (b) GO_LiCl at low magnification, (c) GO_$LiClO_4$, and (d) GO_$NaClO_4$.

Fig. 2. FTIR spectra of GO_MX samples (a); Raman spectrum of GO_LiCl (b), Raman spectrum of GO_$LiClO_4$ (c), and Raman spectrum of GO_$NaClO_4$ (d).

Fig. 3. C1s XPS spectra and related fit of (a) GO_LiCl, (b) GO_$LiClO_4$, and (c) GO_$NaClO_4$.

Fig. 4. Thermogravimetric (TG) and differential thermogravimetric (DTG) curves of GO_MX samples.

Fig. 5. Cyclic Voltammograms of FePC/GO_MX samples in N_2- (dashed lines) and O_2-saturated (solid lines) phosphate buffer solution.

Fig. 6. (a) AFM micrographs of FePc/GO_LiCl and (b) FTIR Spectra of FePc, FePc/GO_LiCl, and GO_LiCl samples.

Fig. 7: XPS spectra of GO_LiCl_FePc (a) C1s (b) N1s and (c) Fe2p.

Fig. 8. (a) Voltage cycles under a 1 kV external resistance recorded for 550 h from inoculation and (b) cell voltage (E) and power density (PD) of MFCs assembled with FePc/GO_LiCl and Pt/C cathodes and fed with 1 mgL^{-1} sodium acetate in neutral phosphate buffer.

Table Captions

Table 1: Raman parameters for GO_LiCl, GO_$LiClO_4$, and GO_$NaClO_4$ samples.

Table 2: Atomic percentage from XPS C1s fit for GO_LiCl, GO_$LiClO_4$, and GO_$NaClO_4$.

Table 3: Weight loss percentage (wt.%), temperature range (T), and temperature of maximum rate of weight change (T_{MAX}) from TG/DTG analysis of Go_LiCl, GO_$LiClO_4$, and GO_$NaClO_4$.

Table 4: E_{pr} (potential of oxygen reduction peak), $|J_{pr}|$ (peak current density), and C_{DL} (double layer capacitance) for FePc and FePc/GO_MX samples.

Table 5: Atomic percentage from XPS C1s, and N1s fit of FePc/GO_LiCl.

Supplementary Materials

Click here to download Supplementary Materials: Fig S1.tif

Supplementary Materials

Click here to download Supplementary Materials: caption to fig s1.docx